International Research Journal of Engineering and Technology (IRJET) e-ISSN: 2395-0056
Volume: 12 Issue: 10 | Oct 2025 www.irjet.net p-ISSN: 2395-0072

3D Markerless Tracking of a Single Fish: A Clean-Water Baseline and First Aged-Water Comparison

Artham Gupta

Abstract

Most studies of fish behavior rely on single-view 2D tracking, which obscures depth and biases motion metrics. I built a simple 3D pipeline using two orthogonal cameras (front and side) and OpenCV-based markerless centroid tracking to reconstruct per-frame (X, Y, Z) positions of a single fish. From the fused trajectory I computed 3D speed, rolling mean speed, speed autocorrelation, 3D voxel occupancy (3×3×3), normalized spatial entropy, and path tortuosity (straightness index and turning-angle statistics). In a clean-water baseline the fish showed broad occupancy (entropy = 0.936 on a 0–1 scale) and a right-skewed speed distribution (mean = 1157 px/s; median = 273 px/s). A first comparison in aged water (same fish, same setup) showed higher central tendency of speed (median = 696 px/s; +155%) but lower spatial entropy (0.698; −25%), suggesting steadier cruising within a reduced spatial envelope. Turning-angle histograms indicated more 60–90° reorientations and fewer extreme U-turns in aged water; straightness index remained low in both conditions. These are pilot results (n = 1 per condition, pixel units), but the code and parameters are transparent and reproducible. The pipeline supports future multi-session statistics, calibration to cm/s, and hypothesis tests on speed, occupancy, entropy, tortuosity, and autocorrelation.

Key Words: fish behavior, water quality, 3D tracking, OpenCV, two-view fusion, entropy, tortuosity

1. INTRODUCTION

Fish are often used as bio-indicators of aquatic environmental conditions due to noticeable changes in their movement patterns and activity levels with changes in water quality [1][2]. For example, the depletion of dissolved oxygen or the buildup of common pollutants such as ammonia can lead to observable shifts in how fish swim, feed, or the areas of the tank within which they spend their time [3][4]. Therefore, researchers have found an accurate link between fish behavior and real-time water quality. Specifically, a reduction in overall activity and feeding, or displays of stressful behavior in poor water conditions make fish natural "monitors" of water quality [4][5]. This is significant because early detection of suboptimal water conditions through motion and behavior analysis could benefit aquaculture by allowing quick intervention [1][6].

For this research's purpose we define clean water as dechlorinated tap water with TDS levels under 300, whereas aged water refers to originally clean water which has degraded in quality through natural accumulation of metabolic waste products (like ammonia or nitrite) over time. Although aged, cycled water contains beneficial bacteria, it may have lower dissolved oxygen levels and higher waste that stresses fish if not well-maintained [7]. We clarify that in this study "aged" water has been in a tank through one full cycle and contains natural wastes to safe levels, as confirmed through frequent multi-faceted water quality tests.

Existing literature emphasizes that even minor alterations in the quality of water can affect the behavior of fish. Most studies focus on extreme cases that show high pollution or poor water conditions can cause fish to be lethargic, feed less, and even avoid certain areas [6]. For example, elevated ammonia concentrations can damage fish gills, increase lethargy, and reduce feeding activity [3][4]. Moreover, increased turbidity (cloudiness) of water due to suspended particles can impair visual sensing in fish, which can further contribute towards increasing foraging time and reducing feeding success rates [8][9]. Additionally, even low to moderate turbidity in aquariums has shown to change school patterns and predatory escape since fish rely heavily on vision to coordinate and avoid threat [10], with one study showing that turbidity above ~9 NTU significantly decreased the prey capture success of dace and significantly affected energy expenditure while feeding [8]. While this is true for many species, some can tolerate moderate levels of turbidity without an immediate breakdown in behavior. For example, stickleback shoals have been observed to remain cohesive in their groups even under certain turbid conditions [11], which indicates that the effect of turbidity can vary by species and context. Overall, however, most literature suggests that small fish are particularly sensitive to water quality, and exhibit reduced activity as well as altered spatial preference under poor water conditions [6]. While most studies have focused on extreme pollutants, there is a relative knowledge gap in studies of how an individual small fish's behavior changes due to moderate alterations of water quality, which are more realistic for artificial aquariums [6].

Single-view 2D tracking can misrepresent aquatic behavior by flattening depth and introducing projection bias. Recent advances in computer vision and deep learning have enabled us to track animal movement without attaching any physical markers [12][13]. DeepLabCut utilizes deep learning through neural networks for pose estimation across frames [12], achieving near human tracking accuracy across diverse species with minimal training data. This technology has several advantages: it's non-invasive, requires regular video, and can even track small-scale movements [14]. In our particular context, DeepLabCut and similar methods have successfully analyzed locomotion and posture in fish. For example, a study by Wu et al. used DeepLabCut to analyze the detailed kinematics of fish while swimming, demonstrating that the tool could reliably extract swim speeds and fin movements [15]. Another project combined DeepLabCut with other tracking algorithms to follow multiple zebrafish and quantify their behavior and anxiety-induced responses. Together, these applications highlight modern pose-tracking's potential for aquatic analysis even in complex scenes [16]. Furthermore, DeepLabCut's multi-animal extension allows the user to maintain the identity of individual fish in groups and even handle infrequent occlusions, a crucial aspect in studying social behavior [16]. Additionally, techniques like optical flow integration can improve tracking stability in videos with noise or poor visibility [17].

This work presents a minimal two-camera, OpenCV-only pipeline to reconstruct 3D trajectories of a single fish in an aquarium, establish a clean-water baseline, and provide a first comparison in aged water. The goal is reproducible metrics rather than exhaustive modeling; all computations are in pixel units with clear limitations noted.

2. METHODS

Two orthogonal cameras recorded the same fish simultaneously (front and side). Per-frame centroids were extracted with OpenCV, temporally aligned, and fused under an orthographic assumption to yield (X, Y, Z) positions in pixels.

OpenCV centroid of the largest moving blob per frame (background-subtraction + morphology). Frame rate: 30 fps. Views were synchronized with a fixed offset; axis mapping and required flips are documented in code. Fusion used per-frame timestamps; when both views were valid, X and Y came from the front view and Z from the side view. No temporal smoothing was applied. Videos were segmented into 5-minute chunks for time-resolved summaries. We did not use DeepLabCut for this study; all tracking used OpenCV centroid detection; DLC is cited as related work.

Metrics: (i) speed (3D) and 30-s rolling mean; (ii) unbiased autocorrelation of speed up to 5 s lag; (iii) 3×3×3 occupancy + normalized spatial entropy; (iv) tortuosity via 60-s straightness index (displacement / path length) and 3D turning angles with a 10% minimum-speed threshold.

Ethics: Non-invasive observation of a single aquarium fish under routine husbandry; no stimuli or handling during trials; educational setting with mentor oversight.

3. RESULTS

3.1 Clean-water baseline (single session)

The clean-water baseline established characteristic patterns of exploratory behavior across multiple 3D metrics. The 3D trajectory (Fig. 1) showed broad spatial coverage with repeated wall passes and extensive depth usage, consistent with healthy tank exploration. Color variation across the path indicated frequent vertical transitions throughout the session.

Mean velocity over time (Fig. 2) exhibited cyclical patterns with peaks marking brief burst movements separated by slower cruising phases. The 30-s rolling window effectively smoothed frame-level noise while preserving multi-minute trends. The speed distribution (Fig. 3) was strongly right-skewed, with mean speed of 1157.3 px/s, median of 272.5 px/s, and 95th percentile of 5385.6 px/s. This distribution reflects characteristic stop-and-go swimming behavior with many low-speed frames and occasional high-speed bursts.

Speed autocorrelation analysis (Fig. 4) revealed short-term temporal structure: positive correlation at brief lags indicated that once the fish accelerated, it maintained elevated speed for several hundred milliseconds before decelerating. Correlation decayed toward zero by approximately 3–5 seconds, suggesting limited long-range periodicity in the baseline condition.

Spatial occupancy analysis using a 3×3×3 voxel grid (Figs. 5–7) demonstrated non-uniform but broad coverage patterns. The XY marginal highlighted preferred lateral-vertical zones; XZ revealed sustained wall-following behavior; and YZ indicated mid-depth preference with secondary usage of shallow and deeper regions. Overall 3D spatial entropy reached 0.936 on a 0–1 scale (Fig. 8), indicating extensive exploration rather than confinement. Per-chunk entropy values ranged from 0.68 to 0.91, confirming consistent spatial distribution throughout the session.

Tortuosity analysis revealed highly meandering movement patterns. The rolling straightness index (Fig. 9) remained near zero (≈0.01–0.05) across the entire session, indicating that within most 60-second windows, the fish traveled long path lengths but ended near its starting position. This pattern

is consistent with wall-following loops and frequent boundary reversals. The turning-angle distribution (Fig. 10) was heavily concentrated at small values (0–10°) representing straight cruising segments, with a secondary peak near 170–180° indicating frequent near-U-turns at boundaries. Per-chunk straightness values (Fig. 11) remained consistently low across all 5-minute segments, confirming that tortuous movement characterized the entire baseline session.

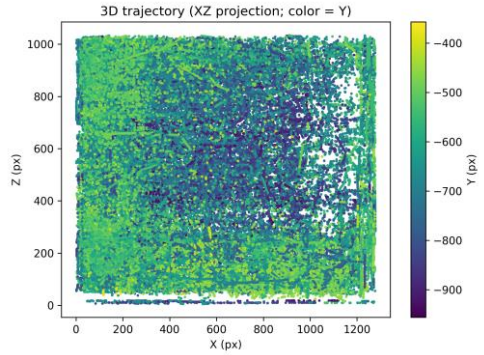

Fig. 1. 3D trajectory (XZ projection; color = Y).

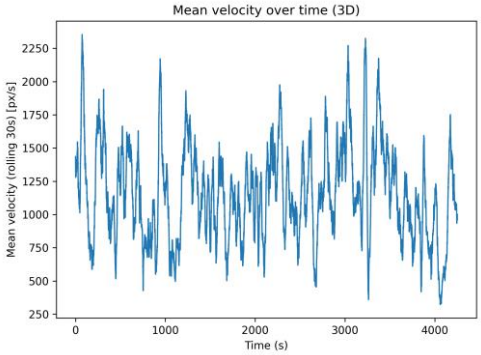

Fig. 2. Mean velocity over time (30-s rolling).

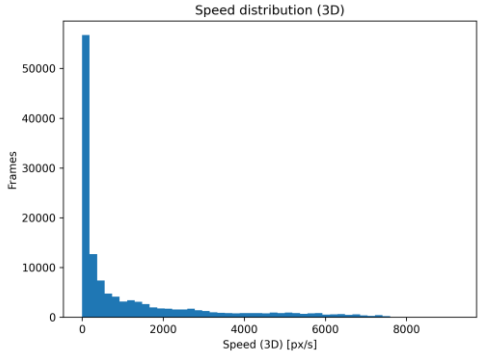

Fig. 3. Speed distribution (3D).

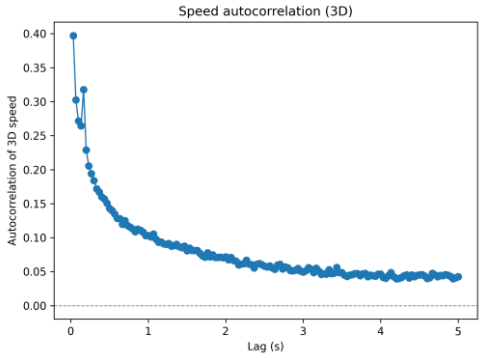

Fig. 4. Autocorrelation of 3D speed (0–5 s).

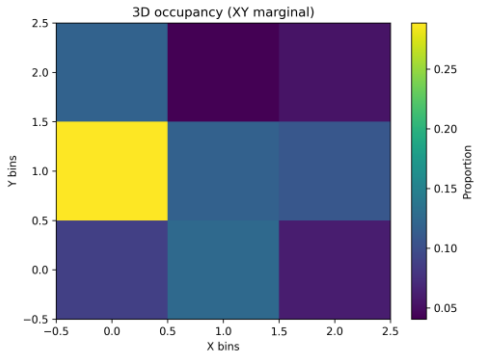

Fig. 5. 3D occupancy heatmap (XY marginal).

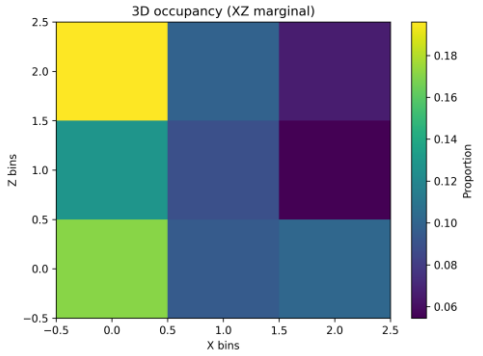

Fig. 6. 3D occupancy heatmap (XZ marginal).

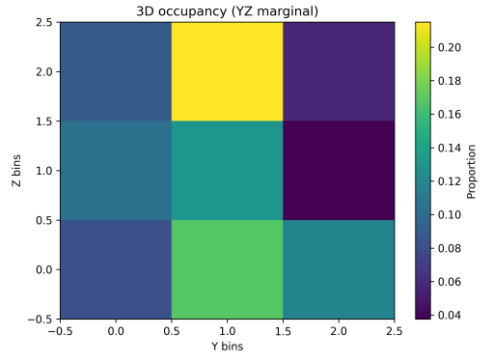

Fig. 7. 3D occupancy heatmap (YZ marginal).

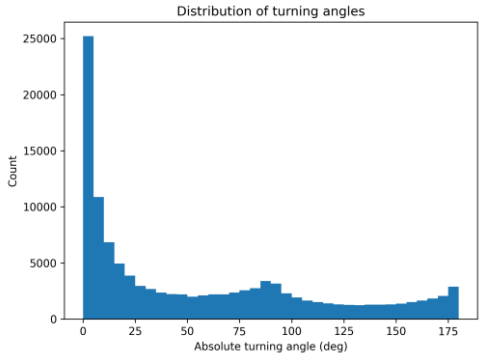

Fig. 10. Distribution of absolute turning angles (3D).

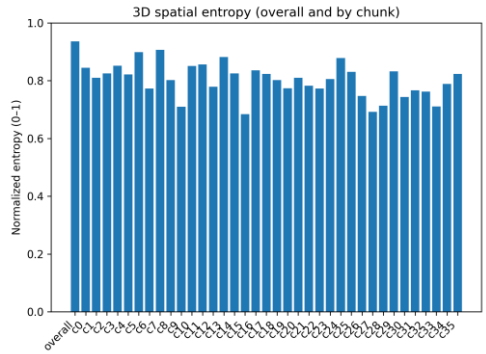

Fig. 8. Normalized spatial entropy overall and per 5-min chunk (overall = 0.936).

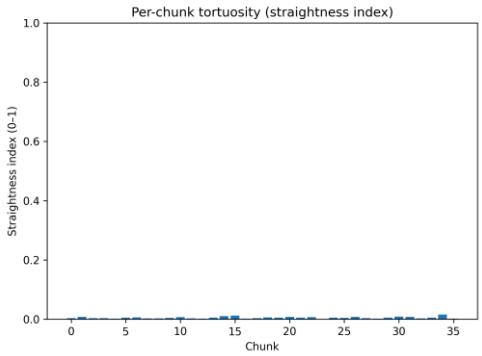

Fig. 11. Tortuosity per 5 min chunk.

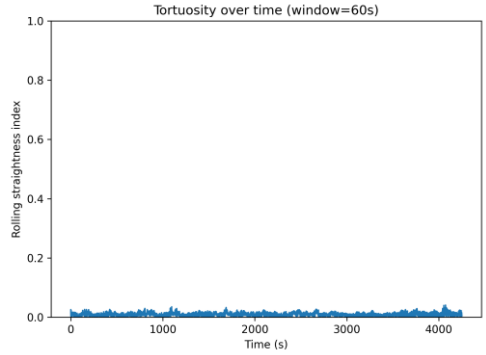

Fig. 9. Rolling straightness index (60-s window).

3.2 Aged-Water Comparison (Same Fish, Same Setup)

The aged-water condition produced notable shifts in movement patterns relative to the clean-water baseline, particularly in spatial distribution and speed characteristics while maintaining similar tortuosity profiles.

The 3D trajectory in aged water (Fig. 2, aged) showed markedly reduced spatial extent compared to clean water. Visual inspection revealed more concentrated movement in specific regions rather than the broad tank-wide coverage observed in clean conditions. This spatial restriction was quantified through occupancy analysis: hexbin density plots (Figs. 3–5, aged) showed stronger localization with distinct "hotspots" of high occupancy, contrasting sharply with the more uniform distribution in clean water.

Spatial entropy decreased substantially in aged water to 0.698 (−25.4% relative to clean water's 0.936), confirming the visual impression of reduced spatial exploration (Fig. 12, aged). This compression of the spatial envelope suggests the fish restricted movement to preferred zones under suboptimal water conditions.

Speed dynamics showed a paradoxical pattern: while spatial usage decreased, central speed tendency increased. The aged-water median speed was 696 px/s (+155% relative to clean water's 273 px/s), indicating faster sustained movement within the reduced spatial range. Mean velocity over time (Fig. 6, aged) showed elevated baseline speeds with continued burst behavior. The speed distribution (Fig. 7, aged) retained its right-skewed character but with a shift toward higher central values and a distinct secondary mode around 4000–5000 px/s, suggesting more frequent moderate-to-high speed swimming.

Speed autocorrelation patterns (Fig. 8, aged) remained qualitatively similar to clean water, with rapid initial decay indicating preserved short-term temporal structure in movement despite the changed water conditions.

The most striking contrast emerged in vertical distribution. While clean-water occupancy showed mid-depth preference with substantial usage of all depth zones, aged-water occupancy (Figs. 9–11, aged) revealed strong concentration in upper regions (higher Z bins in XZ marginal, upper-middle bins in YZ marginal). The XY marginal showed pronounced asymmetry with dominant occupancy in the left-front quadrant. This vertical shift and horizontal localization together produced the substantial entropy reduction.

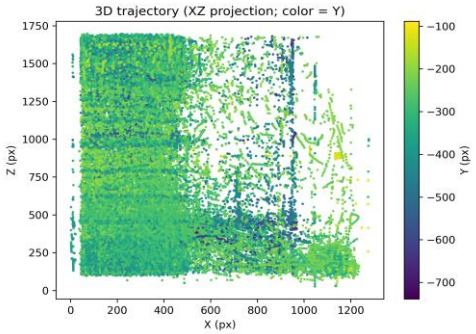

Fig. 12. 3D trajectory (XZ projection; color = Y).

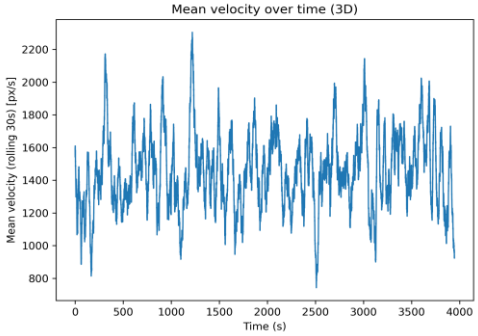

Fig. 13. Mean velocity over time (30-s rolling).

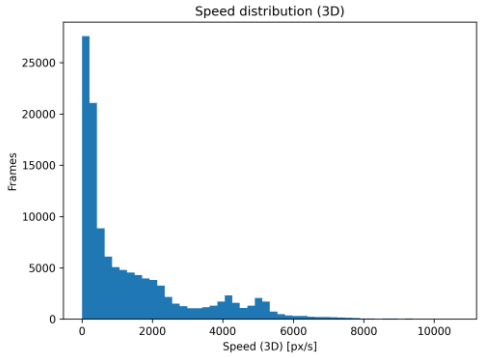

Fig. 14 Speed distribution (3D).

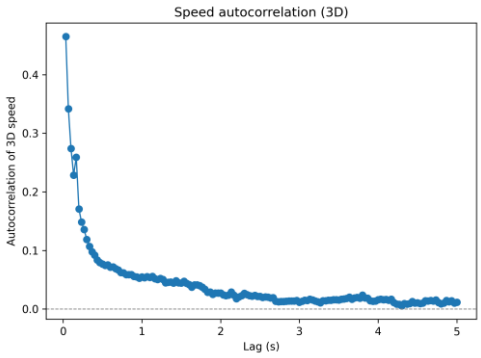

Fig. 15 Autocorrelation of 3D speed (0–5 s).

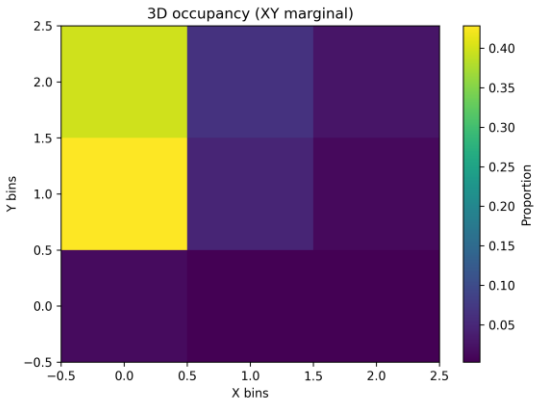

Fig. 16. 3D occupancy heatmap (XY marginal)

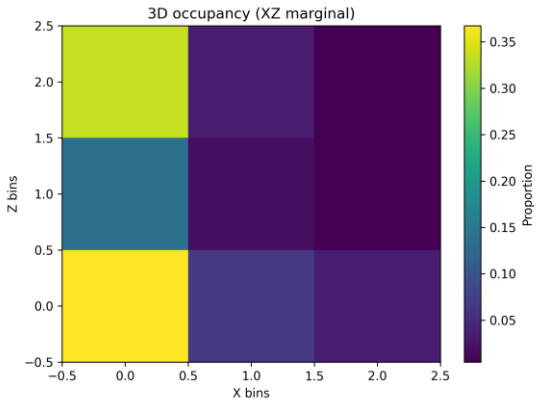

Fig. 17. 3D occupancy heatmap (XZ marginal).

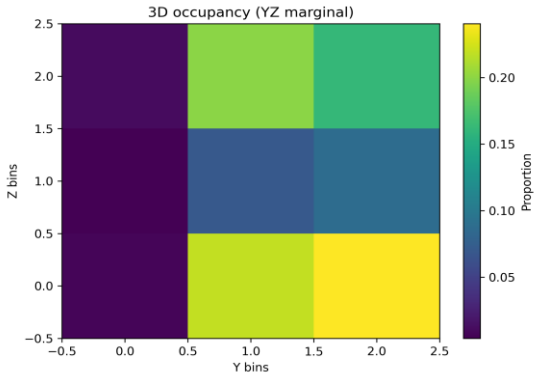

Fig. 18. 3D occupancy heatmap (YZ marginal).

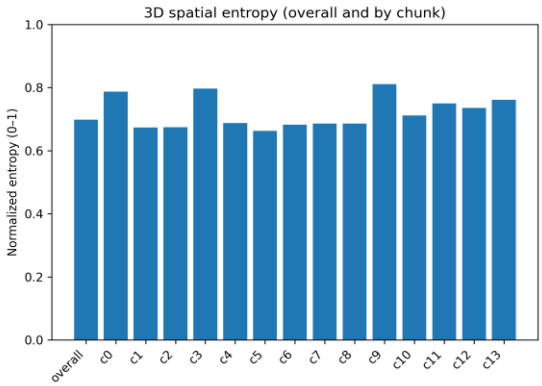

Fig. 19. Normalized spatial entropy overall and per 5-min chunk.

3.3 Tortuosity and Turning Behavior: Condition Comparison

Despite marked differences in speed and space use, tortuosity metrics remained remarkably consistent across conditions. Rolling straightness index time series (Fig. 14) overlaid for both conditions showed nearly identical patterns, with both remaining near zero throughout their respective sessions. Per-chunk straightness values (Fig. 15) showed no systematic difference between clean and aged water, with both conditions maintaining consistently low values (< 0.02 for most chunks).

Turning-angle distributions provided nuanced insights into this preserved tortuosity (Figs. 12–13, comparison). Both conditions showed the characteristic bimodal pattern with peaks at small angles (0–10°) and near 180°. However, subtle shifts were evident: the stacked histogram (Fig. 17) revealed that aged water produced relatively more turns in the 60–90° range and fewer extreme U-turns (170–180°) compared to clean water. The violin plot comparison (Fig. 18) confirmed similar median turning angles (≈50–55°) but showed aged water had a slightly compressed distribution in the high-angle range.

These results indicate that while aged water substantially altered where and how fast the fish moved, it did not fundamentally change the tortuous, loop-based character of movement. The fish continued to execute meandering paths with frequent directional changes in both conditions, though with modified turning-angle composition in aged water.

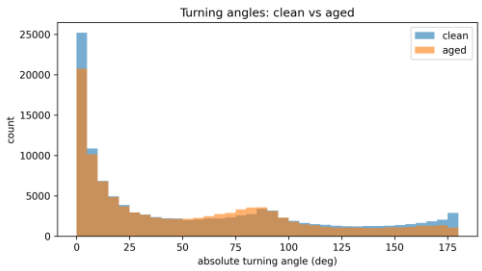

Fig. 20. Turning-angle histogram: clean vs aged.

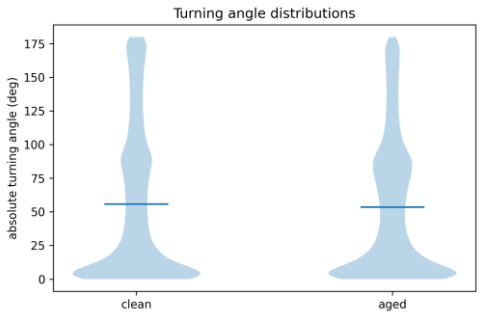

Fig. 21. Turning-angle violin: clean vs aged.

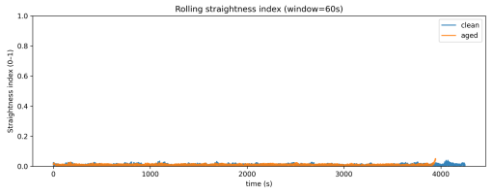

Fig. 22. Rolling straightness index over time: clean vs aged.

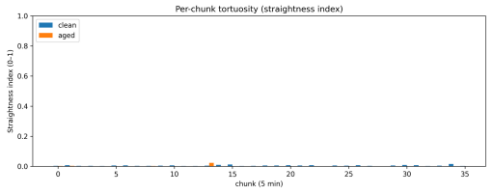

Fig. 23. Per-chunk straightness index by 5-min chunk: clean vs aged.

4. DISCUSSION

4.1 Principal findings (clean vs. aged)

This study established a 3D, two-view, OpenCV-only baseline for a single guppy in clean water and then repeated the same protocol in aged water. Three robust patterns emerged:

Higher central speed but reduced space use in aged water. Median 3D speed increased from 272.5 px/s (clean) to 695.7 px/s (aged; +155%), while normalized 3D spatial entropy dropped from 0.936 to 0.698 (−25%). Mean speed rose from 1157.3 to 1451.9 px/s (+25%), total distance from 4.94×10^6 to 5.73×10^6 px (+16%), and the 95th-percentile speed slightly decreased (−5.7%). *Interpretation:* the fish cruised faster but within a narrower spatial envelope (Figs. 12–19 vs. Figs. 1–8).Temporal structure remained short-range. Speed autocorrelation decayed within ~3–5 s in both conditions (Figs. 4 and 15), indicating brief "memory" in swimming speed with no long-period oscillation.

Tortuosity stayed low in both conditions. The straightness index (SI; displacement/path length) was near zero throughout (Figs. 22–23), indicating loop-rich, meandering paths. Turning-angle statistics kept the familiar bimodal shape (many small turns; some near-U-turns), with aged water showing relatively more 60–90° reorientations and fewer 170–180° flips (Figs. 20–21).

Together, these results suggest that aged water shifted *where* and *how steadily* the fish moved, but not the *movement style*: paths remained tortuous and burst-and-cruise dynamics persisted.

4.2 How these patterns fit prior work

The entropy reduction in aged water aligns with reports that sub-optimal quality can constrain exploration and alter vertical distribution [1], [6]. The increase in median speed is compatible with two non-exclusive mechanisms noted in the literature: (i) surface-seeking or localized cruising under lower dissolved oxygen or mild irritants (faster movement within a smaller volume) [1], [7], and (ii) stress-linked hyperactivity without long, tank-spanning traversals [6]. Our occupancy maps and voxel entropy (Figs. 16–19) show exactly that compression of space use, while the 95th-percentile speed did not rise—hinting that the fish *cruised more* rather than *dashed faster*. Because we did not log chemistry in this pilot, these mechanisms remain hypotheses to be tested, not conclusions.

The short-lag autocorrelation mirrors typical stop-and-go patterns reported in animal tracking studies, where momentum carries across several hundred milliseconds but dissipates rapidly thereafter. The finding that tortuosity and SI profiles were unchanged is consistent with a movement strategy dominated by wall-following loops in a rectangular tank—behavior that persists even as the spatial envelope shrinks.

A key contribution is the two-camera, 3D fusion with no deep-learning pose model. By constructing a per-frame (X,Y,Z) trajectory via synchronized front/side centroids, we avoid depth-projection artifacts that can inflate speed and distort occupancy in 2D. The differences we observe (higher median speed but lower entropy in aged water) are therefore less likely to be analysis artifacts and more likely to reflect real volumetric behavior. This makes the metrics (speed distribution, voxel occupancy/entropy, turning-angle statistics, SI) suitable candidates for condition-classification in future datasets.

4.3 Limitations

n = 1 per condition; single species and individual. These are pilot effects; inferential statistics would be inappropriate at this stage.

Pixel units and orthographic assumption. Without calibration to cm and a refraction model, absolute kinematics are approximate. Still, within-setup comparisons (clean vs. aged) remain meaningful.

No water chemistry logs. We cannot tie behavior to dissolved oxygen, ammonia, nitrite/nitrate, or turbidity. This is the biggest blocker to mechanistic claims.

Tracking biases. OpenCV centroid tracking can be affected by reflections, air bubbles, and background changes. We mitigated this with morphology and consistent lighting, but subtle bias is possible.

Time-of-day/activity state. Although sessions were similar in length, circadian state or feeding history could confound central tendency of speed.

5. CONCLUSION

This study demonstrates a minimal, transparent two-view OpenCV pipeline for 3D markerless tracking of a single aquarium fish and applies it to a clean-water baseline with a first comparison in aged water. By synchronizing orthogonal views under an orthographic assumption and computing volumetric metrics—3D speed (and rolling mean), speed autocorrelation, 3×3×3 voxel occupancy with normalized entropy, straightness index, and 3D turning angles—we obtain interpretable summaries of locomotion that avoid the projection biases of 2D analyses.

In the clean-water session the fish exhibited broad volumetric use (entropy 0.936), a right-skewed speed distribution (mean 1157 px/s, median 273 px/s), short-lag speed memory (autocorrelation decaying within ~3–5 s), and highly tortuous paths (low straightness). In the aged-water session (same fish, same setup) the central tendency of speed increased (median +155%, mean +25%) while spatial entropy decreased (−25%), and turning-angle structure shifted toward more 60–90° reorientations with fewer near-180° reversals. Together, these patterns suggest a behavioral signature of aged water characterized by steadier cruising within a reduced spatial envelope, rather than faster sprints or broader exploration.

The approach is practical for classroom and low-resource labs: it runs on commodity hardware, exposes all parameters, and produces figures that map cleanly onto biological questions about where, how fast, and how animals move in 3D. At the same time, conclusions are necessarily cautious: n=1 per condition, pixel units (no cm calibration), orthographic fusion without refraction modeling, and no concurrent water-chemistry logs. These are the key threats to generalization.

Next steps are clear and actionable: (i) replicate (≥3 sessions per condition, counterbalanced timing); (ii) calibrate to cm (and report speeds in cm/s or body-lengths/s); (iii) log chemistry (DO, temperature, pH, ammonia/nitrite/nitrate, turbidity) to anchor mechanisms; (iv) pre-register primary endpoints (median speed, voxel entropy, SI, angle-band proportions, ACF decay) and statistical tests; and (v) run robustness checks (alternate voxel grids, speed-threshold sensitivity, ACF normalization). With these additions, the same 3D pipeline can deliver statistically supported, mechanistic insights into how routine water-quality changes reshape individual fish behavior.

ACKNOWLEDGEMENT

The author thanks the mentor for guidance and the school for supporting the educational research setting.

REFERENCES

[1] I. Kuklina, A. Kouba, and P. Kozák, "Real-time monitoring of water quality using fish and crayfish as bio-indicators: A review," Environmental Monitoring and Assessment, vol. 185, no. 6, pp. 5043–5053, 2013. DOI: 10.1007/s10661-012-2924-2

[2] Y. Huang, R. Pang, X. Li, W. Li, Z. Yang, D. Wang, and K. Dong, "Ecology health evaluation system based on fish movement behavior response," Water, vol. 15, no. 23, p. 4066, 2023. DOI: 10.3390/w15234066

[3] D. J. Randall and T. K. N. Tsui, "Ammonia toxicity in fish," Marine Pollution Bulletin, vol. 45, no. 1-12, pp. 17–23, 2002. DOI: 10.1016/S0025-326X(02)00227-8

[4] P. Soler, M. Faria, C. Barata, E. García-Galea, B. Lorente, and D. Vinyoles, "Improving water quality does not guarantee fish health: Effects of ammonia pollution on the behaviour of wild-caught pre-exposed fish," PLoS ONE, vol. 16, no. 8, e0243404, 2021. DOI: 10.1371/journal.pone.0243404

[5] A. S. Abangan, D. Kopp, and R. Faillettaz, "Artificial intelligence for fish behavior recognition may unlock fishing gear selectivity," Frontiers in Marine Science, vol. 10, p. 1010761, 2023. DOI: 10.3389/fmars.2023.1010761

[6] K. Zhang, Z. Ye, M. Qi, W. Cai, J. L. Saraiva, Y. Wen, et al., "Water quality impact on fish behavior: A review from an aquaculture perspective," Reviews in Aquaculture, vol. 17, no. 1, pp. 1–27, 2024. DOI: 10.1111/raq.12985

[7] E. Sanders and S. C. Farmer, "Aquatic models: water quality and stability and other environmental factors," ILAR Journal, vol. 60, no. 2, pp. 141–149, 2019. DOI: 10.1093/ilar/ilaa008

[8] R. M. Zamor and G. D. Grossman, "Turbidity affects foraging success of drift-feeding rosyside dace (Clinostomus funduloides)," Transactions of the American Fisheries Society, vol. 136, no. 1, pp. 167–176, 2007. DOI: 10.1577/T05-301.1

[9] G. S. Bilotta and R. E. Brazier, "Understanding the influence of suspended solids on water quality and aquatic biota," Water Research, vol. 42, no. 12, pp. 2849–2861, 2008. DOI: 10.1016/j.watres.2008.03.018

[10] B. R. S. Figueiredo, R. V. Granzotti, L. F. Fiori, C. L. Nieman, E. Benedito, and P. A. Piana, "Cascading effects of predation risk under high organic and inorganic turbidity: Impacts on individuals and shoals of a mesopredator fish," Aquatic Ecology, vol. 54, no. 3, pp. 855–868, 2020. DOI: 10.1007/s10452-020-09787-0

[11] H. E. A. MacGregor and C. C. Ioannou, "Shoaling behaviour in response to turbidity in three-spined sticklebacks," Ecology and Evolution, vol. 13, no. 6, e10134, 2023. DOI: 10.1002/ece3.10134

[12] A. Mathis, P. Mamidanna, K. M. Cury, T. Abe, V. N. Murthy, and M. W. Mathis, "DeepLabCut: markerless pose estimation of user-defined body parts with deep learning," Nature Neuroscience, vol. 21, no. 9, pp. 1281–1289, 2018. DOI: 10.1038/s41593-018-0209-y

[13] T. D. Pereira, D. E. Aldarondo, L. Willmore, M. Kislin, S. S. Wang, M. Murthy, and J. W. Shaevitz, "Fast animal pose estimation using deep neural networks," Nature Methods, vol. 16, no. 1, pp. 117–125, 2019. DOI: 10.1038/s41592-018-0234-5

[14] K. Wei and K. P. Kording, "Behavioral tracking gets real," Nature Neuroscience, vol. 21, no. 9, pp. 1146–1147, 2018. DOI: 10.1038/s41593-018-0215-0

[15] X. Wu, S. Yang, Z. Cai, R. Song, and S. Fan, "Measurement of fish motion parameters based on DeepLabCut," in Proceedings of the 2024 IEEE 19th Conference on Industrial Electronics and Applications (ICIEA), 2024, pp. 970–975. DOI: 10.1109/ICIEA61579.2024.10664666

[16] J. Lauer, M. Zhou, S. Ye, W. Menegas, S. Schneider, T. Nath, et al., "Multi-animal pose estimation, identification and tracking with DeepLabCut," Nature Methods, vol. 19, no. 4, pp. 496–504, 2022. DOI: 10.1038/s41592-022-01443-0

[17] X. Liu, T. Yu, X. Zhao, Z. Wang, G. Tien, and J. Zhao, "OptiFlex: Multi-frame animal pose estimation combining deep learning with optical flow," Frontiers in Cellular Neuroscience, vol. 15, p. 621252, 2021. DOI: 10.3389/fncel.2021.621252